Multiresonance Measurement Method for Microwave Microscopy

Roman Joffe, Reuven Shavit, *Senior Member, IEEE*, and Eugene Kamenetskii

***Abstract*— Nondestructive tests in microwave frequencies for dielectric parameters evaluation with high spatial resolution have a great significance in many fields of material science. In this paper, we present a new method for the dielectric parameter characterization based on the displacement of the multiresonance spectrum of the magnetostatic (MS) oscillations in a thin-film ferrite disk due to loading by a dielectric sample. The effect is manifested by shifting and widening of the MS spectrum that is dependent on the relative permittivity of the sample. The correlation between the MS spectrum characteristics is used in a postprocessing analysis to enhance the separability of noisy data and thereby increase the measurement accuracy. The experimental and numerical results have shown the ability to accurately evaluate the dielectric parameters of the load sample under consideration. The simplicity of the measurement in a wide range of operating frequencies along with nondestructive sensing with a subwavelength resolution of 100 μm complies with the current requirements of scanning microwave microscopy.**

***Index Terms*— Dielectric measurement, microscopy, microwave measurement.**

I. Introduction

MICROWAVE methods and equipment for noninvasive sensing with high spatial resolution are necessary and promising for fields such as nondestructive tests, defects' detection in microelectronic industry, local characterization of dielectric materials, and medical diagnostics [1]–[3]. The existing electromagnetic techniques for materials characterization can be classified into the following categories: transmission-line techniques, free-space techniques, and resonant techniques. All of these methods have their disadvantages and limitations. The transmission line techniques require prior preparation of the embedded samples [4]. The free-space techniques require the use of very large samples, which are placed between special antennas with lenses [5]. In the resonant techniques, the sample is a part of the resonator and must have a specific shape determined by the cavity [6], [7]. The main drawbacks of these methods are that they are destructive and the obtained spatial resolution for identifying any artifact in the sample is limited by the measurement wavelength. To overcome these limitations, nondestructive and noncontact measurement techniques with subwavelength resolution are needed.

Synge [8] was the first to develop a scanning optical microscope, which used evanescent near fields as probing fields. When a pointlike field source is brought in close proximity to the sample, the evanescent field is still strong enough to substantially interact with the sample, thereby allowing measurement at a resolution surpassing the diffraction limit. Further this concept led to the development of near-field microscopy using evanescent microwave fields. Near-field microwave microscopy can be classified into broadband and narrow-band resonant systems. Broadband characterization systems typically use electromagnetic waveguides with an open end or a narrow slot as a near-field source to determine the changes of the system reflection coefficient as a result of the loading sample [9]–[11]. In resonant systems, the scanning probe couples the energy to the microwave cavity. Usually, the microwave cavity used is a quarter-wavelength resonator such as coaxial, microstrip, or stripline [12], [13]. As a general rule, resonant systems are more sensitive because the signal-to-noise ratio (SNR) in a resonator increases with the resonator quality factor (Q-factor). Thus, they are very efficient in a narrow frequency band for which they are designed. The use of electrically long transmission line resonator allows generating a quasi-continuous set of resonances over a frequency band to be exploited in order to have high sensitivity measurements. However, in practice, only few resonant modes are effectively excited and matched to the measurement system [14].

Both in broadband and resonant microwave microscope systems, the spatial resolution is determined by the physical sizes of the probes or slots, and therefore the obtained spatial resolution is significantly lower than the wavelength. The state of the arts of the near-field scanning microwave microscopy (SMM) in terms of spatial resolution and accuracy are the hybrid systems of the near-field microwave reflectometric measurements with standard scanning probe techniques with the nanometric resolution. The key point of these systems is the unique combination of accuracy and speed of vector network analyzer (VNA) along with the scanning capability of the atomic force microscopy and the probe-sample control of scanning tunneling microscopy [15]–[18]. Recently, first commercially available tool of near-field SMM has been introduced by Agilent [19], which has made a huge contribution to the research of biology, semiconductors, and material science in nanoscales [20]–[25]. Furthermore, the

Manuscript received April 24, 2016; revised December 21, 2016; accepted December 26, 2016. Date of publication March 20, 2017; date of current version July 12, 2017. The Associate Editor coordinating the review process was Dr. Sergey Kharkovsky.

R. Joffe is with the Department of Electrical and Computer Engineering, Ben Gurion University of the Negev, Beer Sheva, 8410501, Israel, and also with the Department of Electrical and Electronics Engineering, Shamoon College of Engineering, Beer Sheva 84100, Israel (e-mail: ioffr1@gmail.com).

R. Shavit and E. Kamenetskii are with the Department of Electrical and Computer Engineering, Ben Gurion University of the Negev, Beer Sheva, 8410501, Israel.

Color versions of one or more of the figures in this paper are available online at http://ieeexplore.ieee.org.

Digital Object Identifier 10.1109/TIM.2017.2674338

trend of miniaturization also had an impact on the SMM. The possibility of the integration of near-field microwave sensor together with the high-resolution scanning system on a single embedded chip represents the state of the arts in the field of the development of SMM [26], [27].

Despite of the impressive spatial resolution achieved by the use of the advanced scanning techniques, the operational principle of the microwave sensing in SMM systems almost has not been improved. In the resonant SMM systems, the operation principle is based on the perturbation method [28]. The coupling of the sample to the resonator affects the stored energy within the resonator. The changes in the stored energy within the resonator as a result of the dielectric load are translated into a change of the resonance frequency and the Q-factor of the resonator. Since the permittivity of the material is a complex value, its real and imaginary components are related to the stored energy and the losses within the material. Consequently, for the evaluation of the inhomogeneity of the material dielectric constant, the analysis of the resonance frequency shift is important, while for the material conductivity value, the Q factor is important [17]. However, when the sample encounters high losses, we cannot make a clear distinction between the components that affect the stored energy in the resonator. The parameters are highly coupled and any attempt to separate them negatively affects our understanding of the physical meaning of the problem.

Accurate measurement of high losses materials requires increasing the SNR of the microscope. In order to increase the SNR of the near-field microwave microscopy, both the Q-factor of the resonator and the sensitivity of the probe must be maximized [29], [30]. Thus, a high-quality resonator coupled to the optimized probe is essential for high accurate measurement. A possible way to improve the SNR of the sensor is to perform the measurement at a number of frequencies, which enables to reach high sensitivity and accuracy of the measurement over a large dynamic range. Moreover, it provides richer information about the characteristic of the sample, which allows the implementation of advanced algorithms for noise filtering, immunity to external interference, and improvement of detection capabilities.

Recent studies have shown that in thin-layer ferrite disk with magnetic-dipolar-mode (MDM) oscillations, a rich spectrum of resonance frequencies with high Q-factor is excited. Strong energy concentration and unique topological structures of the near field originated from the MDM resonator allow effective measurement of the dielectric parameters [31]. A thin metal wire, placed above the ferrite disk, localizes the near fields originated from the disk and transfers their unique field topology to the tip of the wire and thereby allows the scanning ability with subwavelength resolution [32], [33]. In the proposed method, the dc magnetic field external parameter is used to set the resonant frequencies of the ferrite disk. This feature enables to achieve high sensitivity at the required frequency without any modification of the sensor. Accordingly, the proposed method bridges the gap between the broadband and narrow-band resonant systems using the flexibility of controlling the operational frequency along with high immunity to measurement noise. Consequently, the implementation of the SMM in the proposed method with a ferrite disk as a resonator is novel and attractive.

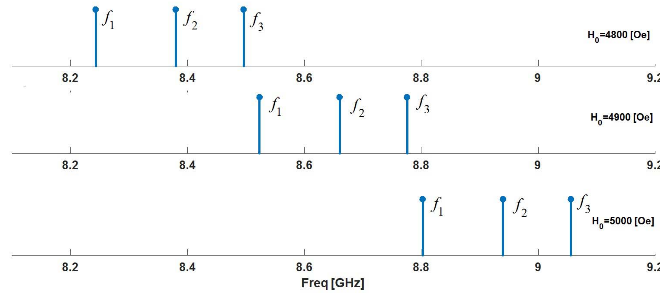

Fig. 1. Analytically calculated resonance frequencies of a ferrite disc resonator. An analysis was made for a disk with radius of 1.5 mm, thickness of 50 μm, and M_S of 1880 G for three values of bias dc magnetic field $H_0 = 4800$, 4900, and 5000 Oe.

In this paper, we present a novel dielectric measurement technique based on the simultaneous analysis of two MDM resonant frequencies. The relative position of the resonant frequencies expands the performance of the data processing. The ability of accurate measurement for a wide range of permittivity values and precise homogenity evaluation of the load sample in a broad frequency band with subwavelength spatial resolution makes the proposed technique attractive and unique.

In measurement setups based on the sensitivity of the resonances to the dielectric sample loading, the variation of the resonance bandwidth is used to determine the tanδ of the sample. However, in the proposed measurement method, we use only the spectral positions of the MDMs' peaks and not their shapes (bandwidth). In any case, in the proposed setup, the evaluation of tanδ is problematic due to the high Q-factor of the resonances generated by the ferrite disk in the system, which significantly degrade the tanδ computation accuracy, and therefore, we did not concentrate on this objective. Consequently, our focus in the proposed system is on improving the accuracy of the dielectric constant evaluation.

II. Dielectric Load Effect on MDM Spectrum

The impact of the dielectric load on the MDM spectrum is a well-observed phenomenon both numerically and experimentally [31], [32], [34]. However, the full theoretical model of the interaction has some complex and unexplained aspects. The very existence of the magnetostatic (MS) potential wave function ($\mathbf{H} = -\nabla\psi$) is due to the assumption of neglecting the displacement current in Maxwell equations [35], [36]. This assumption immediately raises the question about the role of the dielectric load in an MS problem, due to the fact that there is no place for permittivity in MSs. Therefore, any attempt to illustrate the loading effect of the sample on the MDMs of the ferrite disk using an equivalent circuit with lumped elements has no physical meaning.

The analytical calculation of MDM spectrum of the ferrite disk resonator and their classification to radial, azimuthal, and thickness modes was made and numerically validated in [37] and [38]. Fig. 1 illustrates the calculated MDM spectrum for the main thickness mode and for the first three

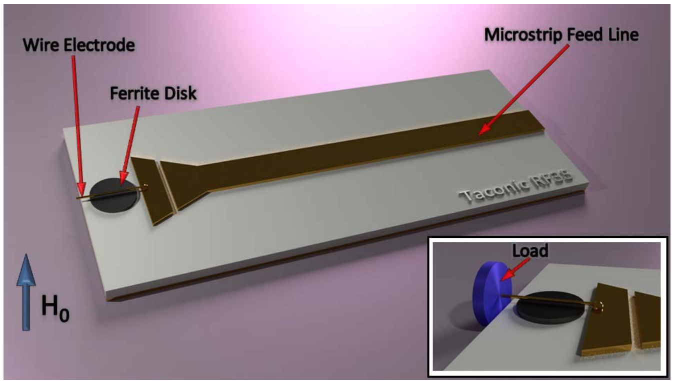

Fig. 2. Geometry of a microwave microstrip structure (sensor) with normally magnetized ferrite disk and wire electrode. The inset shows the tip–sample coupling.

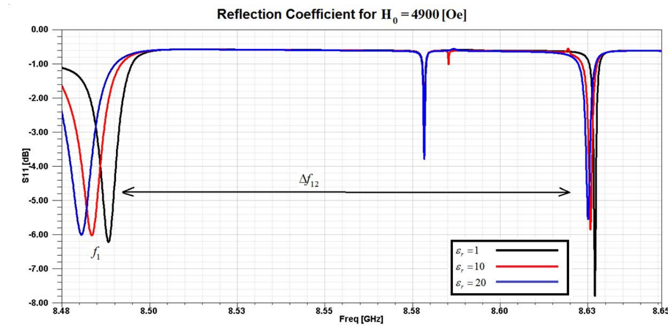

Fig. 3. Frequency characteristics of the reflection coefficient for the MS spectrum for different dielectric loadings (HFSS numerical simulation data).

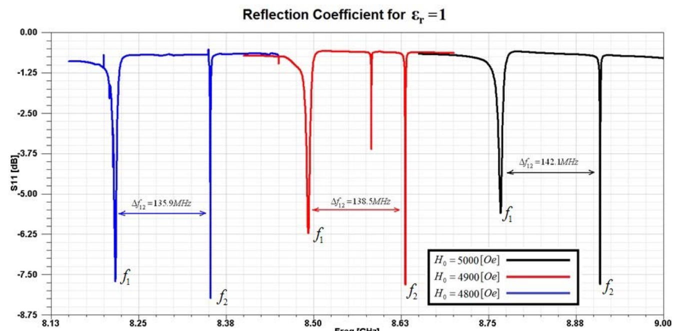

Fig. 4. Frequency characteristics of the reflection coefficient for the MS spectrum and different amplitudes of the external dc magnetic field (HFSS numerical simulation data).

radial modes calculated for Bessel functions of order $m = 1$. The spectrum obtained for a disk with radius of 1.5 mm, thickness of 50 μm, and M_S of 1880 G for three values of bias dc magnetic field $H_0 = 4800$, 4900, and 5000 Oe. From Fig. 1, one can see that the spectral location of the MDMs is dependent on value of external dc magnetic field and can be tuned by it.

Previously, several attempts were made by the authors to theoretically describe the interaction model of the dielectrics loading on the MDM spectrum due to orbital momentum, the secondary mechanical torque, and the topological surface magnetic current [31], [32], [34]. However, these models give only the physical interpretation to the problem. For full analysis of the interaction between the dielectric load and the MDM in the ferrite disk, it is necessary to calculate full electromagnetic problem. Such a problem was solved numerically by the finite-element methods [39], [40]

The ANSYS HFSS software allows numerical computation of the MDM spectral characterization in a ferrite disk. Fig. 2 shows the geometry of an embedded ferrite disk in a microstrip circuit that allows local measurement with subwavelength resolution. The substrate of the microstrip is made from Taconic RF-35 ($\varepsilon_r = 3.5$) with a thickness of 1.52 mm. The width of the microstrip line is 3.3 mm ($Z_0 = 50\ \Omega$). The metallic wire electrode has a diameter of 140 μm and a length of 5 mm. The tip of the wire extends 1 mm beyond the dielectric substrate margin. The YIG ferrite disk diameter is 3 mm, and its thickness is 50 μm with a magnetic saturation of Ms = 1880 G. The external magnetic field is oriented in the normal direction of the disk as shown in Fig. 2. The tip of the wire distance to the sample is 50 μm. In [32] and [33], it has been shown that the wire electrode localizes the ME fields near the tip of the wire. In addition, it has been shown that the unique structure of the localized ME fields exist only on the region of the wire and sharply decays as we move further away from its surface. Numerical simulations have shown that the spatial resolution of the sensor is approximately 100 μm (order of the wire radius), and in addition, the observed azimuthal rotation of the localized ME fields vanishes 300 μm inside the load sample. Therefore, one can assume that the penetration ability of the sensor is approximately 300 μm.

In the simulation of the problem, we have used various types of cylindrical dielectric loads ($\varepsilon_r = \{1,\ 3,\ 10,\ 20,\ 30,\ 50,\ 75,\ 100\}$) and three different magnitudes of external magnetic fields ($H_0 = \{4800,\ 4900,\ 5000\}$ [Oe]). Fig. 3 shows the HFSS results of the reflection coefficient (S_{11}) of the sensor for dielectrics loads with $\varepsilon_r = \{1,\ 10,\ 20\}$ when the external magnetic field is $H_0 = 4900$ Oe. f_1 is the frequency of the first mode, and Δf_{12} is the spectral distance between the second and first modes for each of the loads. In Fig. 3, one can observe that the resonance frequencies of the MS modes are inversely proportional to the dielectric constant of the loads. However, the spectral sensitivity to the dielectric load of the first mode is higher than that of the second mode. Therefore, in addition to shifting of the spectrum, we are witnessing a phenomenon of widening of the spectrum as a result of the dielectric load. Fig. 4 shows simulation results of the reflection coefficient S_{11} for an unloaded ($\varepsilon_r = 1$) sensor and different values of external dc magnetic field $H_0 = \{4800,\ 4900,\ 5000\}$ [Oe].

In Fig. 4, one can see that the spectral distance between the first and second modes (Δf_{12}) is directly proportional to the magnitude of the external dc magnetic field. The conclusion that can be drawn from Figs. 3 and 4 is that for each value of dielectric sample, we will get a unique Δf_{12} curve. The data presented in Fig. 5 are obtained from the simulation results of the relation between the first and second MS modes, and it shows the $\Delta f_{12}(f_1)$ curves for various dielectric values. The data presented in Fig. 6 are obtained from the data

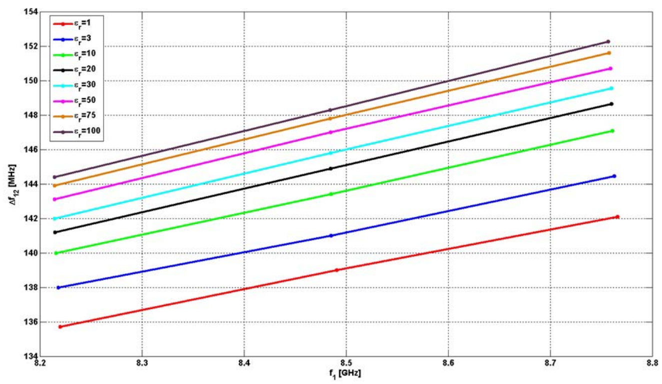

Fig. 5. Δf_{12} as a function of f_1 for various dielectric loads (HFSS numerical simulation data).

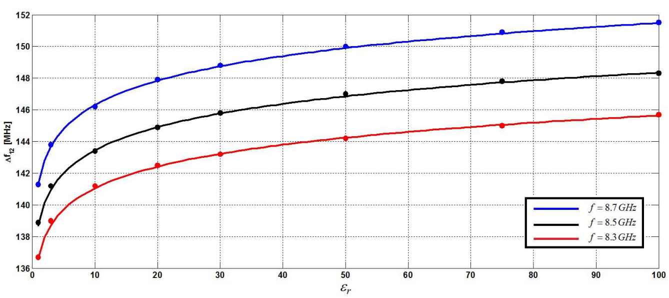

Fig. 6. Δf_{12} as a function of ε_r (HFSS numerical simulation data).

presented in Fig. 5, and it shows the relation between dielectric constant (ε_r) and Δf_{12} for various frequencies. Based on the data presented in Fig. 6, one can note that there is an exponential relation between Δf_{12} and ε_r. This relation can be described empirically by

$$\Delta f_{12}(\varepsilon_r) = \alpha(\varepsilon_r{}^{\beta}) \tag{1}$$

where α is a coefficient proportional to the spectral distance between the first and the second radial MDMs of the unloaded system and β is a dimensionless coefficient. The expression in 1 characterizes only the described ferrite disk resonator shown in Fig. 2, for others dimensions and parameters of the resonator the equation should be recalculated.

III. Calibration Process

The proposed functional relation outlined in (1) based on the spectral analysis can be used for the measurement of the sample homogeneity and its absolute dielectric constant. However, for determination of the parameters α and β in (1), calibration of the system is necessary. To measure the sample homogeneity, the calibration process requires a number of statistical measurements of the sample with different values of the external dc magnetic field. The range of the required magnetic fields amplitudes should satisfy the range of the measurement frequencies. The results of the calibration could be described by the $\Delta f_{12}(f_1)$ trend line and its variance. Any deviations from the trend line can be considered as a nonhomogeneity of the sample.

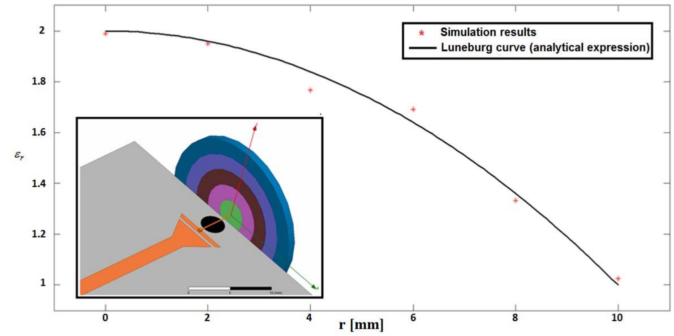

Fig. 7. ε_r as a function of the radius r for the Luneburg lens based on simulation results with HFSS software. The inset shows the geometry of the structure (HFSS numerical simulation data).

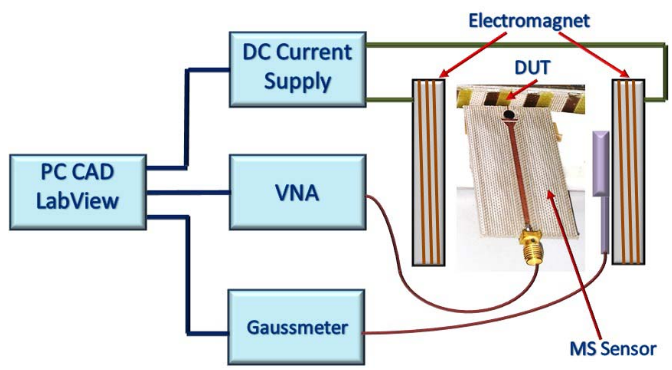

Fig. 8. Block diagram of the experimental setup.

In the case of dielectric constant absolute value measurement, the calibration process should be slightly different and includes two stages. In the first stage, it is necessary to measure Δf_{12} of the unloaded system, while in the second stage, we repeat the Δf_{12} measurement of the loaded system with known samples. This way enables us to calculate the coefficients α and β in (1). It is important to note that the values of Δf_{12} must correspond to the same f_1 (frequency of the first mode) throughout the whole process of calibration and measurement. After the calibration, it is possible to estimate the dielectric constant of any unknown sample simply by measuring its Δf_{12} and use of (1).

As a validation test for the MS sensor performance, a simulation of a planar Luneburg lens [41] has refractive index dependent on the radius r given by $n = (\varepsilon_r)^{1/2} = (2 - (r/R)^2)^{1/2}$ with $R = 1$ cm being the lens radius. Fig. 7 shows the postprocessing results. The Luneburg lens simulation results illustrate the ability to measure the absolute value of the dielectric constants as well as the variation of the dielectric constant along the lens.

IV. Experimental Measurement

In Fig. 8, one can see the block diagram of the experimental setup. The sensor (see Fig. 2) and the sample (DUT) are parts of a three-axis linear transmission system that ensures noncontact sensing with a tip–sample distance of 50 μm when the tip–sample distance controlled manually by linear stage and optical microscope. The external electromagnet provides the necessary magnitude of the dc magnetic field required for the ferrite disk. The input and output signals are sampled with the VNA while the signal processing, control, and monitoring of the measurement procedure are performed using LabVIEW (PC-CAD).

In our analysis, we set the central frequency of VNA to 8.5 GHz with a span of 400 MHz and an IF filter bandwidth of 1 KHz. The reason of the selected central frequency is due to the fact that the excitation microstrip device is matched at this frequency. The span of 400 MHz allows us convenient analysis of the changes in spectral characteristics due to the loads. Another implication of the frequency span choice (400 MHz) using this setup is that in the proposed method, the results are valid only for nondispersive materials in the measurement frequency span. The tradeoff between the measuring speed and the noise reduction is determined by the bandwidth of the IF filter. Choosing of IF bandwidth as 1 KHz allows measuring the spectrum of MDMs with an SNR of 20 dB.

In the proposed measurement method, we use only the spectral location of the MDMs of the ferrite disk resonator. For this reason, special preprocess of calibration has been developed. In the first stage, we have to measure and save the reflection coefficient of the system without applying a dc magnetic field. Thereby, there are no excitations of MDMs in the ferrite disk. The saved data consist only from the reflection of the microstrip system, cables, connectors, and the hardware of the VNA. After the supply of the dc magnetic field to the ferrite disk, the MDMs are excited. The subtraction of the saved data from the measured gives only the MDMs peaks on zero baseline. The proposed preprocess of calibration allows calibrating the system without any disconnection of the cables and the use of any special calibration kits and thereby simplifies the measurement procedure.

A. Dielectric Constant Measurement Setup

Equation (1) shows the exponential relation between widening of the MS spectrum (Δf_{12}) and the dielectric constant (ε_r) of the sample. However, for the estimation of ε_r from Δf_{12} measurement, the calibration of the sensor is necessary. For the calibration process, we used a sample with dielectric constant $\varepsilon_r = 100$ (K-100; TCI Ceramics). The results of the experiment were measured and obtained at 8.5 GHz. The selection of the measurement frequency is done by variation of the external dc magnetic field magnitude, which stabilizes the frequency of the first MS mode (f_1) at 8.5 GHz. Consequently, the operating frequency of the system can change from 1 to 20 GHz without any additional changes in the system (as long as the system is matched and the received signal is stable).

In the first calibration stage, we have measured the unloaded system. In this case, the widening of the spectrum was $\Delta f_{12} = 139.5$ MHz. In the second stage of the calibration, the sample with dielectric constant $\varepsilon_r = 100$ was used. For this case, the widening of the spectrum was $\Delta f_{12} = 145.87$ MHz. For the calculation of the coefficients α and β, $\Delta f_{12}(\varepsilon_r = 1)$ and $\Delta f_{12}(\varepsilon_r = 100)$ were substituted into (1) resulting in $\alpha = 139.5$ and $\beta = 0.0097$. Accordingly, the relation between Δf_{12} and ε_r is $\Delta f_{12}(\varepsilon_r) = 139.5\,\varepsilon_r^{0.0097}$. During the measurement process of Δf_{12}, it is necessary to control f_1 to be constant at 8.5 GHz. Some known dielectric samples with $\varepsilon_r = 3.5$ (Taconic RF-35), $\varepsilon_r = 4.3$ (FR4), $\varepsilon_r = 30$ (K-30; TCI Ceramics), and $\varepsilon_r = 50$ (K-50; TCI Ceramics) were measured, and their dielectric constants were computed using (1) for validation purposes. The measurement results are summarized in Table I. From Table I one can see that the measurement errors between the proposed method and the conventional techniques are less then 10%.

TABLE I
MEASUREMENT RESULTS AT FREQUENCY OF 8.5 GHz

Material	ε_r (Data sheet)	Δf_{12} [MHz]	$\hat{\varepsilon}_r$ (Measured)	Error (%)
Taconic RF35	3.5	141.11	3.25	7.14
FR4	4.3	141.46	4.18	2.79
K-30	30	144.31	32.9	9.66
K-50	50	144.83	47.8	4.4

TABLE II
COMPARISON BETWEEN MEASUREMENT AND NUMERICAL DATA

ε_r	Δf_{12} [MHz] (Experimental)	Δf_{12} [MHz] (Numerical)
30	144.31	145.9
50	144.83	146.9
100	145.87	148.3

Table II shows some experimental measurement results in comparison with the corresponding numerical results (see Fig. 5).

The differences between the numerical and experimental results are due to the influence of environment conditions (temperature stability, current drift, etc.) and the value of the demagnetization factor of the ferrite disk, which may be in error due to non-uniformity of the magnetic field in the disk. All these factors are not taken into account in the numerical simulation. In the numerical simulation, the ferrite disk is uniformly magnetized; actually, there is a demagnetization factor of the disk that along with the inhomogeneity of the external dc magnetic field leads to the inhomogeneous magnetic field in the disk. In the experiment, we waited until the MDM spectrum became stable.

B. Increase in SNR Using Multiresonance Sensing

Multiresonant sensing while maintaining the bandwidth is equivalent to an increase in the SNR (the ratio of the expected signal value to the noise variance) of the measurement. In addition, this kind of sensing enables signal postprocessing methods using shifting and widening of the resonance peaks. In Fig. 9, one can see the f_1 and Δf_{12} measurement data for two different materials (Taconic RF35 and FR4). For each material, 50 samples were taken.

Fig. 9(a) shows the position of the first mode frequency that was set at 8.5 GHz throughout the entire measurement process. Fig. 9(b) shows the spectral distance between the first and second modes. One can see that the average value of Δf_{12} for FR4 is higher than the average value for Taconic RF35. However, the measurement data are noisy and it is impossible

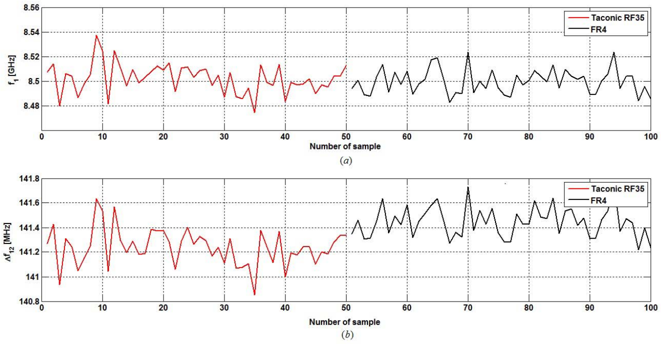

Fig. 9. Experimental results: the first 50 samplings were taken for Taconic RF35 and the second 50 samplings were taken for FR4. (a) f_1. (b) Δf_{12}.

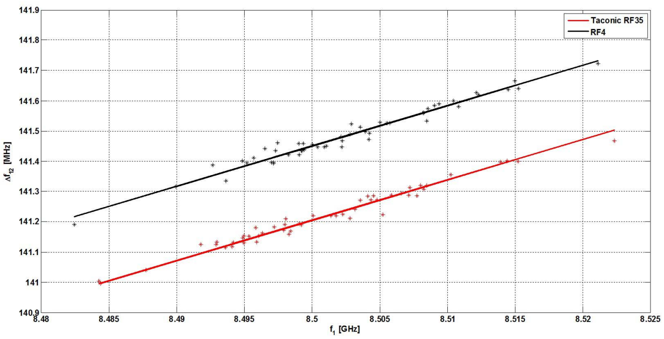

Fig. 10. $\Delta f_{12}(f_1)$ curves for Taconic RF35 and FR4 (experimental results).

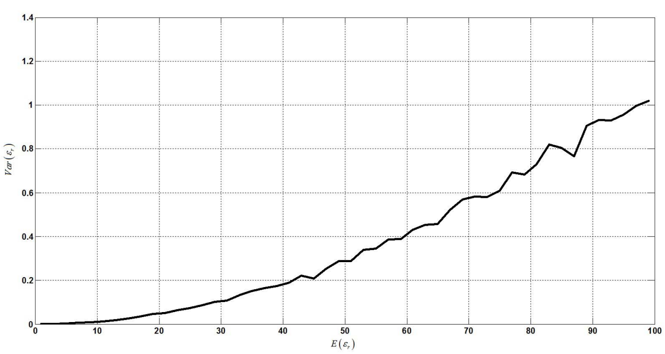

Fig. 11. Expected value and the variance of dielectric constant.

to identify a threshold that gives 100% probability of detection. Despite the fact that the SNR of the measurement is low, one can see that exists a correlation between the noise in f_1 and Δf_{12}. The correlative noise in the measurements of f_1 and Δf_{12} in fact is enriching the data of $\Delta f_{12}(f_1)$ curve. Therefore, this makes it possible to increase the separability of the data, which is equivalent to an increase in the SNR measurement. Fig. 10 shows the measurement data and its trend lines in $(f_1, \Delta f_{12})$ space.

From Fig. 10, one can see that after the implementation of the spectral analysis method, it is possible to select the threshold that improves the overall performance. The variance of Δf_{12} relative to the trend line is about 200 KHz. To estimate the accuracy of the dielectric constant measurement, it is necessary to substitute the variance of Δf_{12} into (1). Fig. 11 shows the error (variance) as a function of the expected value of the dielectric constant given that the variance of the Δf_{12} is 200 KHz. From Fig. 11, one can see that the measurement error is less than 1%.

V. Conclusion

In this paper, multiresonant sensing is used to increase the performance of permittivity measurements of the sample. The setup realization is based on the spectral analysis of an MS sensor, using a thin-layer ferrite disk resonator with MDM oscillations and metallic wire electrode as a concentrator of ME fields. The analysis of the influence of dielectric load on the MDM spectrum showed that there is a correlation between the widening of the MDM spectrum (Δf_{12}) and the dielectric constant of the load. The data postprocessing method based on spectral analysis has been proposed and confirmed both numerically and experimentally. Finally, it has been shown that the sensor is able to identify an error in the material homogeneity with an accuracy of less than 1% and measuring the absolute value of the dielectric constants in a wide range of frequencies at a subwavelength resolution of 100 μm.

References

[1] M. Tabib-Azar, P. S. Pathak, G. Ponchak, and S. LeClair, “Nondestructive superresolution imaging of defects and nonuniformities in metals, semiconductors, dielectrics, composites, and plants using evanescent microwaves,” *Rev. Sci. Instrum.*, vol. 70, no. 6, pp. 2783–2792, 1999.

[2] B. T. Rosner and D. W. van der Weide, “High-frequency near-field microscopy,” *Rev. Sci. Instrum.*, vol. 73, no. 7, pp. 2505–2525, 2002.

[3] A. N. Reznik and N. V. Yurasova, “Electrodynamics of microwave near-field probing: Application to medical diagnostics,” *J. Appl. Phys.*, vol. 98, no. 11, p. 114701, 2005.

[4] H. Yue, K. L. Virga, and J. L. Prince, “Dielectric constant and loss tangent measurement using a stripline fixture,” *IEEE Trans. Compon., Packag., Manuf. Technol. B*, vol. 21, no. 4, pp. 441–446, Nov. 1998.

[5] F. H. Wee, P. J. Soh, A. H. M. Suhaizal, H. Nornikman, and A. A. M. Ezanuddin, “Free space measurement technique on dielectric properties of agricultural residues at microwave frequencies,” in *Proc. SBMO/IEEE MTT-S Int. Microw. Optoelectron. Conf. (IMOC)*, Nov. 2009, pp. 183–187.

[6] M. D. Janezic and J. Baker-Jarvis, “Full-wave analysis of a split-cylinder resonator for nondestructive permittivity measurements,” *IEEE Trans. Microw. Theory Techn.*, vol. 47, no. 10, pp. 2014–2020, Oct. 1999.

[7] M. S. Boybay and O. M. Ramahi, “Material characterization using complementary split-ring resonators,” *IEEE Trans. Instrum. Meas.*, vol. 61, no. 11, pp. 3039–3046, Nov. 2012.

[8] E. H. Synge, “A suggested method for extending microscopic resolution into the ultra-microscopic region,” *London, Edinburgh, Dublin Philos. Mag. J. Sci.*, vol. 6, no. 35, pp. 356–362, 1928.

[9] M. Golosovsky and D. Davidov, “Novel millimeter-wave near-field resistivity microscope,” *Appl. Phys. Lett.*, vol. 68, no. 11, pp. 1579–1581, 1996.

[10] A. F. Lann *et al.*, “A cryogenic microwave scanning near-field probe: Application to study of high-T_c superconductors,” *Rev. Sci. Instrum.*, vol. 70, no. 11, pp. 4348–4355, 1999.

[11] C. P. Vlahacos, R. C. Black, S. M. Anlage, A. Amar, and F. C. Wellstood, “Near-field scanning microwave microscope with 100 μm resolution,” *Appl. Phys. Lett.*, vol. 69, no. 21, pp. 3272–3274, 1996.

[12] M. Tabib-Azar, N. S. Shoemaker, and S. Harris, “Non-destructive characterization of materials by evanescent microwaves,” *Meas. Sci. Technol.*, vol. 4, no. 5, p. 583, 1993.

[13] C. Gao, T. Wei, F. Duewer, Y. Lu, and X.-D. Xiang, “High spatial resolution quantitative microwave impedance microscopy by a scanning tip microwave near-field microscope,” *Appl. Phys. Lett.*, vol. 71, no. 13, pp. 1872–1874, 1997.

[14] A. Tselev, S. M. Anlage, Z. Ma, and J. Melngailis, “Broadband dielectric microwave microscopy on micron length scales,” *Rev. Sci. Instrum.*, vol. 78, no. 4, p. 044701, 2007.

[15] M. Tabib-Azar and Y. Wang, “Design and fabrication of scanning near-field microwave probes compatible with atomic force microscopy to image embedded nanostructures,” *IEEE Trans. Microw. Theory Techn.*, vol. 52, no. 3, pp. 971–979, Mar. 2004.

[16] A. Imtiaz, M. Pollak, S. M. Anlage, J. D. Barry, and J. Melngailis, "Near-field microwave microscopy on nanometer length scales," *J. Appl. Phys.*, vol. 97, no. 4, p. 044302, 2005.

[17] A. Imtiaz and S. M. Anlage, "A novel STM-assisted microwave microscope with capacitance and loss imaging capability," *Ultramicroscopy*, vol. 94, nos. 3–4, pp. 209–216, 2003.

[18] M. Farina, D. Mencarelli, A. D. Donato, G. Venanzoni, and A. Morini, "Calibration protocol for broadband near-field microwave microscopy," *IEEE Trans. Microw. Theory Techn.*, vol. 59, no. 10, pp. 2769–2776, Oct. 2011.

[19] W. Han, "Introduction to scanning microwave microscopy mode," Agilent Technol., Inc, Appl. Note 5989-8881EN, 2008.

[20] S. Fabiani *et al.*, "Dual-channel microwave scanning probe microscopy for nanotechnology and molecular biology," in *Proc. IEEE Eur. Microw. Conf. (EuMC)*, Sep. 2010, pp. 767–770.

[21] S. Fabiani *et al.*, "Broadband scanning microwave microscopy investigation of graphene," in *IEEE MTT-S Int. Microw. Symp. Dig.*, Jun. 2011, pp. 1–4.

[22] M. C. Biagi *et al.*, "Nanoscale electric permittivity of single bacterial cells at gigahertz frequencies by scanning microwave microscopy," *ACS Nano*, vol. 10, no. 1, pp. 280–288, 2015.

[23] Y. J. Oh *et al.*, "High-frequency electromagnetic dynamics properties of THP1 cells using scanning microwave microscopy," *Ultramicroscopy*, vol. 111, no. 11, pp. 1625–1629, 2011.

[24] G. Gramse *et al.*, "Quantitative sub-surface and non-contact imaging using scanning microwave microscopy," *Nanotechnology*, vol. 26, no. 13, p. 135701, 2015.

[25] E. Brinciotti *et al.*, "Probing resistivity and doping concentration of semiconductors at the nanoscale using scanning microwave microscopy," *Nanoscale*, vol. 7, no. 35, pp. 14715–14722, 2015.

[26] N. Sarkar, M. Azizi, S. Fouladi, and R. R. Mansour, "Self-actuating scanning microwave microscopy probes," in *IEEE MTT-S Int. Microw. Symp. Dig.*, Jun. 2012, pp. 1–3.

[27] M. Azizi, N. Sarkar, and R. R. Mansour, "Single-chip CMOS-MEMS dual mode scanning microwave microscope," *IEEE Trans. Microw. Theory Techn.*, vol. 61, no. 12, pp. 4621–4629, Dec. 2013.

[28] O. Klein, S. Donovan, M. Dressel, and G. Grüner, "Microwave cavity perturbation technique: Part I: Principles," *Int. J. Infr. Millim. Waves*, vol. 14, no. 12, pp. 2423–2457, 1993.

[29] M. Tabib-Azar, D.-P. Su, A. Pohar, S. LeClair, and G. Ponchak, "0.4 μm spatial resolution with 1 GHz ($\lambda = 30$ cm) evanescent microwave probe," *Rev. Sci. Instrum.*, vol. 70, no. 3, pp. 1725–1729, 1999.

[30] S. Hong, J. Kim, W. Park, and K. Lee, "Improved surface imaging with a near-field scanning microwave microscope using a tunable resonator," *Appl. Phys. Lett.*, vol. 80, no. 3, pp. 524–526, 2002.

[31] M. Sigalov, E. O. Kamenetskii, and R. Shavit, "Electric self-inductance of quasi-two-dimensional magnetic-dipolar-mode ferrite disks," *J. Appl. Phys.*, vol. 104, no. 5, p. 053901, 2008.

[32] R. Joffe, E. O. Kamenetskii, and R. Shavit, "Novel microwave near-field sensors for material characterization, biology, and nanotechnology," *J. Appl. Phys.*, vol. 113, no. 6, p. 063912, 2013.

[33] E. O. Kamenetskii, E. Hollander, R. Joffe, and R. Shavit, "Unidirectional magnetoelectric-field multiresonant tunneling," *J. Opt.*, vol. 17, no. 2, p. 025601, 2015.

[34] E. O. Kamenetskii, R. Joffe, and R. Shavit, "Microwave magnetoelectric fields and their role in the matter-field interaction," *Phys. Rev. E, Stat. Phys. Plasmas Fluids Relat. Interdiscip. Top.*, vol. 87, no. 2, p. 023201, 2013.

[35] A. G. Gurevich and G. A. Melkov, *Magnetization Oscillations and Waves*. Boca Raton, FL, USA: CRC Press, 1996.

[36] D. D. Stancil, *Theory of Magnetostatic Waves*. New York, NY, USA: Springer, 1993.

[37] E. O. Kamenetskii, "Energy eigenstates of magnetostatic waves and oscillations," *Phys. Rev. E, Stat. Phys. Plasmas Fluids Relat. Interdiscip. Top.*, vol. 63, no. 6, p. 066612, 2001.

[38] E. O. Kamenetskii, M. Sigalov, and R. Shavit, "Quantum confinement of magnetic-dipolar oscillations in ferrite discs," *J. Phys., Condens. Matter*, vol. 17, no. 13, p. 2211, 2005.

[39] M. Sigalov, E. O. Kamenetskii, and R. Shavit, "Magnetic-dipolar and electromagnetic vortices in quasi-2D ferrite discs," *J. Phys., Condens. Matter*, vol. 21, no. 1, p. 016003, 2008.

[40] E. O. Kamenetskii, R. Joffe, and R. Shavit, "Coupled states of electromagnetic fields with magnetic-dipolar-mode vortices: Magnetic-dipolar-mode vortex polaritons," *Phys. Rev. A, Gen. Phys.*, vol. 84, no. 2, p. 023836, 2011.

[41] R. K. Luneburg and M. Herzberger, *Mathematical Theory of Optics*. Berkeley, CA, USA: Univ. of California Press, 1964.

Roman Joffe was born in Latvia, U.S.S.R., in 1983. He received the B.Sc. degree in electrical and electronics engineering from the Sami Shamoon College of Engineering, Beer-Sheva, Israel, in 2009, and the M.Sc. degree in electrical and computer engineering from the Ben Gurion University of the Negev, Beer-Sheva, in 2012, where he has been pursuing the Ph.D. degree in electrical and computer engineering since 2012.

His current research interests include microwave sensing and microwave microscopy of dielectric, magnetic, and biological materials and structures.

Reuven Shavit (M'82–SM'90) received the B.Sc. and M.Sc. degrees in electrical engineering from the Technion-Israel Institute of Technology, Haifa, Israel, in 1971 and 1977, respectively, and the Ph.D. degree in electrical engineering from the University of California, Los Angeles, CA, USA, in 1982.

From 1971 to 1993, he was a Staff Engineer and an Antenna Group Leader with the Electronic Research Laboratories, Israeli Ministry of Defense, Tel Aviv, Israel, where he was involved in the design of reflector, microstrip, and slot antenna arrays. He was a part-time Lecturer with Tel Aviv University, Tel Aviv, teaching various antenna and electromagnetic courses. From 1988 to 1990, he was a Principal Engineer with ESSCO, Concord, MA, USA, where he was involved in scattering analysis and tuning techniques of high performance ground based radomes. He is currently a Professor with the Ben-Gurion University of the Negev, Beer-Sheva, Israel, where he is involved in research in microwave components and antennas. His current research interests include the areas of metamaterials, smart antennas, tuning techniques for radomes, and numerical methods for design microstrip, slot, and reflector antennas.

Eugene Kamenetskii photograph and biography not available at the time of publication.